Title

The Effects of an Albumin Binding Moiety on the Targeting and Pharmacokinetics of an Integrin αvβ6-Selective Peptide Labeled with Aluminum [18F]Fluoride

Journal

Molecular Imaging and Biology, 22(6)

ISSN

1536-1632

Authors

Hausner, Sven H
Bauer, Nadine
Davis, Ryan A
et al.

Publication Date

2020-12-01

DOI

10.1007/s11307-020-01500-0

Peer reviewed

HHS Public Access

Author manuscript

Mol Imaging Biol. Author manuscript; available in PMC 2021 December 01.

Published in final edited form as:

Mol Imaging Biol. 2020 December ; 22(6): 1543–1552. doi:10.1007/s11307-020-01500-0.

The Effects of an Albumin Binding Moietyon the Targeting and Pharmacokinetics of an Integrin $\alpha_v\beta_6$-Selective Peptide Labeledwith Aluminum [^{18}F]Fluoride

Sven H. Hausner[1], **Nadine Bauer**[1], **Ryan A. Davis**[2], **Tanushree Ganguly**[1], **Sarah Y. C. Tang**[1], **Julie L. Sutcliffe**[1,2,3]

[1]Division of Hematology/Oncology, Department of Internal Medicine, University of California Davis, Sacramento, CA, USA

[2]Department of Biomedical Engineering, University of California Davis, Davis, CA, USA

[3]Center for Molecular and Genomic Imaging, University of California Davis, Davis, CA, USA

Abstract

Purpose: The $\alpha_v\beta_6$-BP peptide selectively targets the integrin $\alpha_v\beta_6$, a cell surface receptor recognized as a prognostic indicator for several challenging malignancies. Given that the 4-[^{18}F] fluorobenzoyl (FBA)-labeled peptide is a promising PET imaging agent, radiolabeling via aluminum [^{18}F]fluoride chelation and introduction of an albumin binding moiety (ABM) have the potential to considerably simplify radiochemistry and improve the pharmacokinetics by increasing biological half-life.

Procedures: The peptides NOTA-$\alpha_v\beta_6$-BP (**1**) and NOTA-K(ABM)-$\alpha_v\beta_6$-BP (**2**) were synthesized on solid phase, radiolabeled with aluminum [^{18}F]fluoride, and evaluated in vitro (integrin ELISA, albumin binding, cell studies) and *In vivo* in mouse models bearing paired DX3puroβ6 [$\alpha_v\beta_6$(+)]/DX3puro [$\alpha_v\beta_6$(−)], and for [^{18}F]AlF **2**, BxPC-3 [$\alpha_v\beta_6$(+)] cell xenografts (PET imaging, biodistribution).

Results: The peptides were radiolabeled in 23.0 ± 5.7 % and 22.1 ± 4.4 % decay-corrected radiochemical yield, respectively, for [^{18}F]AlF **1** and [^{18}F]AlF **2**. Both demonstrated excellent affinity and selectivity for integrin $\alpha_v\beta_6$ by ELISA ($IC_{50}(\alpha_v\beta_6)$ = 3–7 nM vs $IC_{50}(\alpha_v\beta_3)$ > 10 μM) and in cell binding studies (51.0 ± 0.7 % and 47.2 ± 0.7 % of total radioactivity bound to DX3puroβ6 cells at 1 h, respectively, *vs.* ≤ 1.2 % to DX3puro for both compounds). The radiotracer [^{18}F]AlF **1** bound to human serum at 16.3 ± 1.9 %, compared to 67.5 ± 1.0 % for the ABM-containing [^{18}F]AlF **2**. *In vivo* studies confirmed the effect of the ABM on blood circulation (≤ 0.1 % ID/g remaining in blood for [^{18}F]AlF **1** as soon as 1 h p.i. *vs.* > 2 % ID/g for [^{18}F]AlF **2**

Correspondence to: Julie Sutcliffe; jlsutcliffe@ucdavis.edu.

Electronic supplementary material The online version of this article (https://doi.org/10.1007/s11307-020-01500-0) contains supplementary material, which is available to authorized users.

Conflict of Interest

S. H. Hausner is a co-inventor of intellectual property related to [^{18}F]$\alpha_v\beta_6$-BP.J. L. Sutcliffe is founder of and holds ownership interest (including patents) in Luminance, Biosciences, Inc., and is a co-inventor of intellectual property related to [^{18}F]$\alpha_v\beta_6$-BP. The other authors declare that they have no conflict of interest.

at 6 h p.i.) and higher $\alpha_v\beta_6$(+) tumor uptake (4 h: DX3puroβ6; [^{18}F]AlF **1**: 3.0 ± 0.7 % ID/g, [^{18}F]AlF **2**: 7.2 ± 0.7 % ID/g; BxPC-3; [^{18}F]AlF **2**: 10.2 ± 0.1 % ID/g).

Conclusion: Both compounds were prepared using standard chemistries; affinity and selectivity for integrin $\alpha_v\beta_6$ in vitro remained unaffected by the albumin binding moiety. *In vivo*, the albumin binding moiety resulted in prolonged circulation and higher $\alpha_v\beta_6$-targeted uptake.

Keywords

Peptide; Integrin $\alpha_v\beta_6$; Aluminum [^{18}F]fluoride; Albumin; Albumin binding moiety; Blood circulation; PET imaging

Introduction

Peptide-based radiopharmaceuticals are being developed for diagnosis and therapy, most notably in oncology [1–5]. For positron emission tomography (PET) imaging, the radioisotope fluorine-18 remains a leading choice due to its favorable decay characteristics ($T_{1/2}$ = 110 min; % (β^+) = 97 %; β^+_{max} = 0.64 MeV) along with established prosthetic group radiochemistry including the more recently developed [^{18}F]fluoride-capture reactions [5–8]. For the latter, radiolabeling of chelator-bearing peptides with aluminum [^{18}F]fluoride is particularly attractive because of its simple and widely applicable methodology compatible with commercially available reagents (*viz* NOTA chelators), the high stability of the final radiolabeling moiety, and the possibility to label the same NOTA-peptide with diagnostic or therapeutic radiometals [5, 8–10]. At the same time, a potential challenge for some aluminum [^{18}F]fluoride NOTA-peptide radiotracers remains the increased uptake of radioactivity in the kidneys compared to their counterparts radiolabeled with covalent fluorine-18 prosthetic groups [11–13].

For a radiotracer to reach its full potential, the pharmacokinetic properties, including target specificity, *In vivo* serum stability, circulation time, and clearance characteristics, need to be optimized [2, 13–15]. Peptides typically clear rapidly from the bloodstream *via* the renal pathway which can lead to low uptake in the target tissue (*e.g.*, tumor); furthermore, peptides radiolabeled *via* chelators can be susceptible to trapping of high levels of radioactivity in the kidney, thus limiting their clinical applications [14–17]. Non-covalent binding to plasma proteins has been suggested as a way to address both issues and has been widely studied as part of the general drug development process to assess a drug's absorption, distribution, metabolism, and excretion (ADME) profile [18–24]. Here, the presence of a chemical moiety that binds non-covalently to plasma proteins (commonly to human serum albumin, HSA) is being used to increase circulation time in the blood and facilitate renal recycling. More recently, this use of non-covalent albumin binding moieties (ABMs) is also being leveraged for radiopharmaceuticals, particularly in the form of specific lipophilic functional groups in proximity to carboxylates, or as fragments of albumin dye [25–32].

Here, we present a study evaluating two analogs of [^{18}F]$\alpha_v\beta_6$-BP [33], a 4-[^{18}F]fluorobenzoyl ([^{18}F]FBA)-labeled peptide that is currently in a phase 1 clinical study (NCT03164486). [^{18}F]$\alpha_v\beta_6$-BP selectively targets the cell surface receptor integrin $\alpha_v\beta_6$. This integrin has been recognized as a prognostic indicator for several challenging

malignancies, including breast, pancreatic, gastric, and colon cancers, with high levels of expression linked to poor survival [34–36]. The $\alpha_v\beta_6$-BP peptide analogs NOTA-$\alpha_v\beta_6$-BP (**1**) and NOTA-K(ABM)-$\alpha_v\beta_6$-BP (**2**) share the same integrin $\alpha_v\beta_6$ recognition sequence and were designed for radiolabeling with aluminum [^{18}F]fluoride *via* the NOTA chelator; in addition, **2** also bears a peripheral albumin binding moiety (ABM) attached to the ε-amine of a lysine (Fig. 1). We describe the synthesis and the *in vitro* evaluation (integrin ELISA, serum stability, albumin binding, cell binding, and internalization using the engineered DX3puroβ6 [$\alpha_v\beta_6$(+)] and DX3puro [$\alpha_v\beta_6$(−)] pair of cell lines and pancreatic BxPC-3 [$\alpha_v\beta_6$(+)] cells) and *In vivo* evaluation in mouse models (using paired DX3puroβ6/DX3puro and BxPC-3 tumors; PET imaging, biodistribution).

Materials and Methods

General

Reagents and solvents were purchased from Millipore Sigma (St. Louis, MO, USA), Fisher Scientific (Pittsburgh, PA, USA), or Acros/VWR (Radnor, PA, USA) unless stated otherwise. NovaSyn TGR and NovaSyn TGR R resins were used with 9-Fluorenylmethoxycarbonyl (Fmoc)-protected L-amino acids bearing the following amino acid side-chain protections: 2,2,4,6,7-pentamethyldihydrobenzofuran-5-sulfonyl (Pbf) for arginine, *tert*-butyl ester (O*t*Bu) for aspartic acid, tert-butyl (*t*Bu) for threonine, and trityl (Trt) for asparagine and glutamine; *N*-α−1-(4,4-dimethyl-2,6-dioxocyclohex-1-ylidene)-3-methylbutyl-*N*-ε-Fmoc-L-lysine (ivDde-Lys(Fmoc)-OH) was used to install the albumin binding side chain. Monodisperse Fmoc-amino-PEG-propionic acid (Fmoc-PEG-COOH; FW = 1544.8 g/mol) was purchased from Polypure (Oslo, Norway); 2-(4,7-bis(2-(*tert*-butoxy)-2-oxoethyl)-1,4,7-triazonan-1-yl)acetic acid (NOTA-bis(*tert*-butyl ester)) was purchased from CheMatech (Dijon, France). PETNET Solutions (Sacramento, CA, USA) supplied the [^{18}F]fluoride ion in ^{18}O-water. CHROMAFIX 30-PS-HCO3 cartridges were purchased from ABX (Radeberg, Germany), Sep-Pak C18 Plus cartridges were purchased from Waters (Milford, MA, USA), and Centrifree Ultrafiltration devices were purchased from Millipore Sigma. Dulbecco's modified Eagle medium (DMEM), Roswell Park Memorial Institute (RPMI) 1640 medium, fetal bovine serum (FBS), penicillin-streptomycinglutamine (PSG), and phosphate-buffered saline (PBS) were purchased from Gibco/Thermo Fisher (Waltham, MA, USA). Growth factor-reduced (GFR) Matrigel was purchased from Corning (Corning, NY, USA). A Wizard 1470 γ-counter (Perkin-Elmer, Waltham, MA, USA) was used to count radioactivity in solution, cell binding, and biodistribution samples.

Mass spectrometry analysis was performed at the UC Davis Mass Spectrometry Facility using a matrix-assisted laser desorption ionization time of flight (MALDI TOF) spectrometer (UltraFlextreme; Bruker, Billerica, MA, USA; 4700 Mass Spectrometer; Applied Biosystems/Thermo Fisher) in positive ionization mode using a α-cyano-4-hydroxycinnamic acid or sinapinic acid matrix.

The cell lines have been described previously [37, 38]. Cells were cultured at 37 °C and 5 % CO_2 in medium containing 10 % heat-inactivated fetal bovine serum and 1 % PSG; DMEM containing puromycin (2 μg/ml) was used for the DX3puro and DX3puroβ6 cells, and the

medium for the BxPC-3 cells was RPMI. Integrin expression was confirmed prior to experiments by flow cytometry using a LSRFortessa instrument with FACSDiva software (both Becton Dickinson, Franklin Lakes, NJ, USA) [38].

ELISA

Competitive binding enzyme-linked immunosorbent assays (ELISAs) for integrins $\alpha_v\beta_6$ and $\alpha_v\beta_3$ followed previously described procedures and were analyzed using Prism software (GraphPad Software, La Jolla, CA, USA) [37]. Experiments were run in triplicate, using biotinylated latency-associated peptide (G&P Biosciences, Santa Clara, CA, USA) for $\alpha_v\beta_6$ ELISA and vitronectin (Thermo Fisher) biotinylated using a biotinylation kit (Thermo Fisher) for $\alpha_v\beta_3$ ELISA as competing ligands. Non-fat dry milk powder (Raley's, West Sacramento, CA, USA) was used in place of bovine serum albumin; blocking buffer consisted of PBS containing 0.5 % milk powder (w/v) and 1 % Tween 20 (v/v); conjugate buffer was prepared by adding 0.1 % milk powder (w/v) to wash buffer [37].

Lipophilicity Measurement

Lipophilicity of the radiotracers was determined by the octanol/PBS partitioning method. Experiments were run in quadruplicate for each radiotracer. An aliquot of each formulated radiotracer (50 μl; 75–300 kBq/ml) was diluted with PBS to 500 μl and combined with an equal volume of *n*-octanol in a microfuge tube. The tube was vortexed vigorously for 3 min and then centrifuged (10,000×*g*, 6 min). Equal volumes of each layer (100 μl/each) were withdrawn and transferred in separate tubes for γ-counting. Data for log $D_{7.4}$ are expressed as mean ± standard deviation of the logarithm of the ratio of counts measured in octanol to the counts measured in PBS.

Serum Stability

The stability of the radiotracers was evaluated in mouse serum (Millipore Sigma) or human serum (Millipore Sigma) by incubating serum (0.5 ml) containing the formulated radiotracer (12.5–25 μl, 2–6 MBq) at 37 °C in a sealed microfuge tube. Following incubation, aliquots were withdrawn, serum proteins precipitated, and aliquots of the supernatant analyzed by HPLC as previously described [11].

Albumin Binding

Binding of the radiotracers to serum proteins was evaluated by ultrafiltration using Centrifree Ultrafiltration devices according to the manufacturer's recommendations. Experiments were carried out in quadruplicate. The devices were pre-treated with PBS containing Tween 20 (5 % v/v) [18], followed by triplicate rinses with PBS. An aliquot of each formulated radiotracer in PBS (≤ 25 μl, 20–60 KBq) was thoroughly mixed with 0.5 ml serum at 37 °C in a microfuge tube. The mixture was incubated at 37 °C for 5 min, and an aliquot (50 μl) was transferred to a tube for γ-counting. The remaining sample was transferred to a Centrifree Ultrafiltration device and centrifuged for 40 min at 1500×*g* at ambient temperature (20–24 °C). An aliquot (50 μl) of the filtrate was transferred to a tube for γ-counting. For each radiotracer, a blank was run using 0.5 ml PBS/Tween 20 (5 % v/v) instead of serum ($n = 4$) to determine non-specific binding. Following γ-counting, the

protein-bound radioactivity was calculated by subtracting the counts measured in the filtrate aliquot (*i.e.*, not protein bound) from the counts in the corresponding serum aliquot. The data are expressed as mean ± standard deviation of fraction of radioactivity bound to protein after subtraction of non-specific binding determined in the blank.

Cell Binding and Internalization

Binding of the radiotracers to and internalization into DX3puro, DX3puroβ6, and BxPC-3 cells were determined as previously described [11, 16]. Non-fat dry milk powder (0.5 % w/v in PBS) was used to pretreat the assay tubes to prevent non-specific binding.

In vivo Studies

All animal procedures conformed to the Animal Welfare Act and were approved by the University of California Davis Institutional Animal Care and Use Committee. Female athymic nude mice (Charles River Laboratories; Wilmington, MA, USA) were inoculated subcutaneously with 3×10^6 DX3puro and 3×10^6 DX3puroβ6 cells in DMEM on opposite flanks or with 5×10^6 BxPC-3 cells in DMEM/ Matrigel (1/1 v/v). Studies commenced once tumors reached a maximum diameter of ~ 0.5 cm.

The radiotracers were injected into the tail vein of mice anesthetized with isoflurane in medical grade oxygen (imaging 5–7 MBq/animal; biodistribution 1.5–3.3 MBq/animal) while the injected mass was kept constant at 0.175 nmol per injection (corresponding to 7 nmol/kg for a 25-g mouse) through addition of nonradioactive compound to the radiotracer solution. For imaging, two mice/scan were placed side-by-side in a prone position ($n = 4$ animals total/ radiotracer; anesthesia 1.5–2.0 % isoflurane); PET scans were acquired using an Inveon DPET scanner (Siemens Medical Solutions, Knoxville, TN, USA), and CT scans were obtained with an Inveon SPECT/CT scanner (Siemens); PET scans were static 15 min-scans at 1, 2, and 4 h p.i., and a static 30 min-scan at 6 h p.i. Imaging data were analyzed as previously described using Inveon Research Workplace software (Siemens) [11].

For biodistribution studies, mice were euthanized and dissected 1, 2, and 4 h p.i. ([^{18}F]AlF **1**) or 2, 4, and 6 h p.i. ([^{18}F]AlF **2**; $n = 3$–4 animals/compound/time point). Tissues were collected, rinsed, and radioactivity measured in a γ-counter; calibrated, decay-corrected radioactivity concentrations are expressed as percent of injected dose per gram of sample (% ID/g). For the blocking studies, 8.36 μmol/kg peptide 1 or 2, respectively, was injected intravenously ($n = 2$ animals/tumor model; 75 μl saline solution; [11, 38]) 10 min before administration of the radiotracer. Animals were sacrificed 1 h p.i. (for [^{18}F]AlF **1**) or 4 h p.i. (for [^{18}F]AlF **2**) and tissues handled and analyzed as described above.

For [^{18}F]AlF **2**, a blood sample was obtained with sufficient radioactivity (1.2 MBq) for *In vivo* serum stability analysis 1 h after injection of 37 MBq. The sample was immediately centrifuged (1150×*g*, 10 min) and the serum was isolated. Proteins were precipitated with an equal volume of ethanol and removed by centrifugation (10,000×*g*, 3 min). The protein removal process was repeated with a half-volume of ethanol. The final supernatant was diluted with an equal volume water/TFA (0.05 % v/v)/glacial acetic acid (2 % v/v) for HPLC analysis.

Statistical Analysis

Quantitative data are reported as mean ± standard deviation (SD). Statistical analysis was done using a paired two-tailed Student's *t* tests to evaluate statistical significance, where $P < 0.05$ was considered statistically significant.

Chemistry, radiochemistry, and chromatography methods are provided in the electronic supplementary material.

Results

Chemistry and Radiochemistry

Using standard Fmoc-solid phase chemistry with ivDde-Lys(Fmoc)-OH for installation of the ABM, the NOTA-peptides were obtained in ≥ 95 % purity after HPLC purification; non-radioactive fluorine-19 standards were obtained using $AlCl_3$ and KF in ≥ 95 % purity after HPLC purification (**1**: MS (MALDI) m/z = 5082.8936 $[M + H]^+$, calcd M ($C_{223}H_{417}N_{39}O_{90}$) 5081.9252, 5082.9331 $[M + H]^+$; AlF **1**: MS (MALDI) m/z = 5127.2437 $[M + H]^+$, calcd M ($C_{223}H_{415}AlFN_{39}O_{90}$) 5125.8895, 5126.8974 $[M + H]^+$; **2**: MS (MALDI) m/z = 5683.0165 $[M + H]^+$, calcd M ($C_{247}H_{450}IN_{43}O_{96}$) 5682.0697; 5683.0775 $[M + H]^+$; AlF **2**: MS (MALDI) m/z = 5727.5389 $[M + H]^+$, calcd M ($C_{223}H_{415}AlFIN_{43}O_{96}$) 5726.034; 5727.0418 $[M + H]^+$). The corresponding radiotracers were obtained in a synthesis time of 90–100 min (including HPLC purification) at molar activities > 37 GBq/μmol in 23.0 ± 5.7 % decay-corrected radiochemical yield (dc RCY) and 22.1 ± 4.4 % dc RCY, respectively, for [^{18}F]AlF **1** ($n = 7$) and [^{18}F]AlF **2** ($n = 7$); radiochemical purities were 97.0 ± 1.3 % and 95.4 ± 1.8 %, respectively.

In Vitro Studies

Affinity and selectivity for integrin $\alpha_v\beta_6$ were evaluated by competitive ELISAs against the natural ligands: peptide 1 showed an affinity (IC_{50}) for integrin $\alpha_v\beta_6$ of 7 ± 3 nM, and IC_{50} for 2 was 3 ± 1 nM; for integrin $\alpha_v\beta_3$, no binding was observed at concentrations up to 10 μM (Fig. 2). Binding was also evaluated in cell studies using the integrin $\alpha_v\beta_6$-expressing cell lines BxPC-3 and DX3puroβ6, and the $\alpha_v\beta_6$-null DX3puro control (Fig. 2). For [^{18}F]AlF **1**, binding to DX3puroβ6 cells was 51.0 ± 0.7 % (of total radioactivity) and internalization was 31.6 ± 0.6 % (of total radioactivity); for [^{18}F]AlF **2**, binding was 47.2 ± 0.7 % and internalization was 27.5 ± 1.3 %. For both compounds, binding to DX3puro cells was ≤ 1.2 % (internalization ≤ 0.5 %), resulting in DX3puroβ6/DX3puro-ratios for total binding of 43/1 ([^{18}F]AlF **1**) and 49/1 ([^{18}F]AlF **2**); for internalization, the ratios were 61/1 ([^{18}F]AlF **1**) and 72/1 ([^{18}F]AlF **2**). Using the pancreatic BxPC-3 cells, 45.1 ± 0.7 % binding and 31.5 ± 1.3 % internalization were observed for [^{18}F]AlF **1**, closely matching the data for [^{18}F]AlF **2** of 43.8 ± 0.7 % binding and 31.6 ± 1.1 % internalization.

Albumin binding was determined by ultrafiltration using Centrifree filtration devices; for the ABM-containing [^{18}F]AlF **2**, 54.3 ± 1.3 % and 67.5 ± 1.0 % protein binding were observed for mouse and human serum, respectively, compared to 24.8 ± 1.4 % and 16.3 ± 1.9 %, respectively, for the reference [^{18}F]AlF **1**. Lipophilicity of the compounds was measured by the octanol/PBS partitioning method: log $D_{7.4}$ was − 2.69 ± 0.19 and − 2.20 ± 0.06 for

[^{18}F]AlF **1** and [^{18}F]AlF **2**, respectively. Serum stability was measured in mouse and human serum; in mouse serum at 2 h, [^{18}F]AlF **1** remained 67 % intact and [^{18}F]AlF **2** remained 92 % intact; in human serum at the same time point, the compounds remained ≥ 97 % and ≥ 95 % intact, respectively. Additionally, the serum stability of [^{18}F]AlF **2** was also measured in human serum at 6 h where it was found to remain ≥ 95 % stable.

In vivo Studies

The two radiotracers were evaluated in the cell xenograft tumor mouse models. A comparison of [^{18}F]AlF **1** and [^{18}F]AlF **2** showed greatly reduced elimination from the body for the ABM-containing [^{18}F]AlF **2**. When evaluated during imaging studies, 61.8 ± 5.6 % (dc) of the injected radioactivity remained in the body at 4 h p.i. for [^{18}F]AlF **2**, compared to 21.7 ± 3.4 % for [^{18}F]AlF **1** (Supplementary Figure S1). As illustrated in Fig. 3 for PET images of the paired DX3puroβ6/DX3puro model, [^{18}F]AlF **1** cleared rapidly from the bloodstream, and the highest levels of radioactivity were observed for excretory organs, chiefly the kidneys and bladder (urine); the $\alpha_v\beta_6$-expressing DX3puroβ6 tumor did show contrast compared to the $\alpha_v\beta_6$-negative DX3puro tumor, but the signal remained low throughout for [^{18}F]AlF **1**. By contrast, the ABM-containing [^{18}F]AlF **2** resulted in comparatively higher blood pool signal, which was most pronounced at the early time points. While excretory organs still showed the highest signal, chiefly in the kidneys and bladder (urine), the contrast for the $\alpha_v\beta_6$-expressing DX3puroβ6 tumor increased over time as seen particularly in the 6-h scan. These observations were substantiated when [^{18}F]AlF **2** was carried forward for PET/CT and biodistribution studies in the pancreatic BxPC-3 mouse model; there, the imaging also showed prolonged blood circulation along with strong signal from excretory organs as well as the endogenously $\alpha_v\beta_6$-positive tumor which was clearly visible at all time points (Fig. 4).

Biodistribution studies confirmed these observations for both mouse models (Figs. 5 and 6, Supplementary Tables S1 and S2). The data obtained in the paired DX3puroβ6/DX3puro model showed that ≤ 0.1 % ID/g remained in the blood for [^{18}F]AlF **1** as soon as 1 h p.i. Uptake in the DX3puroβ6 tumor was 2.2 ± 0.5 % ID/g at 1 h and 3.0 ± 0.7 % ID/g at 4 h, alongside ≤ 0.3 % ID/g in the DX3puro tumor at all time points; blocking with non-radioactive peptide reduced uptake in the DX3puroβ6 tumor at 1 h to 0.44 ± 0.04 % ID/g (Δ = − 80 %; P = 0.016; the DX3puro tumor uptake was 0.46 ± 0.04 % ID/g). Highest levels of radioactivity were found in the kidneys (steady at 39 ± 10 to 41 ± 10 % ID/g, respectively, at 1 and 4 h), stomach, and large intestine (both ranging from 5 to 7 % ID/g at all time points), while the liver, muscle, and bone all averaged ≤ 0.9 % ID/g. For [^{18}F]AlF **2**, the level of radioactivity in the blood was 9.9 ± 2.2 % ID/g at 2 h and decreased slowly to 3.7 ± 0.3 % ID/g at 6 h. Uptake in the DX3puroβ6 tumor appeared to trend upward from 7.0 ± 0.5 % ID/g at 2 h to 9.0 ± 1.0 % ID/g at 6 h, while the values for the DX3puro tumor dropped over the same time frame (2.3 ± 0.3 % ID/g to 1.5 ± 0.4 % ID/g); blocking with non-radioactive peptide resulted in a reduction to 2.4 ± 0.4 % ID/g for the DX3puroβ6 tumor (Δ = − 67 %; P = 0.007) when evaluated at 4 h, while uptake in the DX3puro tumor remained steady (2.3 ± 0.2 % ID/g). Highest levels of radioactivity were once again found in the kidneys (49 ± 5 to 68 ± 4 % ID/g from 2 to 6 h) and stomach (18.6 ± 1.5 to 26.0 ± 1.0 % ID/g from 2 to 6 h), followed by the large and small intestines (both ranging from 11 to 17 % ID/g at all time

points); the liver, muscle, and bone all averaged ≤ 3.0 % ID/g. A comparison between the two radiotracers at the 2 and 4 h time points shows that introduction of the albumin binding moiety increased retention in the blood by over two orders of magnitude for [^{18}F]AlF **2** *vs.* [^{18}F]AlF **1**; this prolonged circulation in the blood pool resulted in a greater than two-fold increase for the DX3puroβ6 tumor while the kidneys, in contrast, increased only 1.5-fold (Fig. 5). The introduction of the ABM moiety did also increase uptake in organs of the lower gastro-intestinal tract. For *In vivo* serum stability evaluation of [^{18}F]AlF **2**, the blood sample contained sufficient radioactivity for analysis by HPLC; it revealed that [^{18}F]AlF **2** stayed 77 % intact after 1 h *In vivo* in mouse.

The biodistribution data subsequently obtained with [^{18}F]AlF **2** in the BxPC-3 model showed a continuous increase of uptake in the BxPC-3 tumor from 6.4 ± 0.7 % ID/g at 2 h to 13.6 ± 2.5 % ID/g at 6 h, along with low levels in the pancreas (between 0.8 and 1.2 % ID/g at all time points) and a steady decrease of blood radioactivity levels overtime to 2.4 ± 0.4 % ID/g at 6 h (Fig. 6, Supplementary Table S2). This resulted in tumor-to-organ ratios of 5.7 ± 0.3/1, 12 ±2.1/1, and 10.8 ± 2.9/1 for blood, pancreas, and muscle, respectively; blocking studies at 4 h with non-radioactive peptide resulted in a drop from 10.2 ± 0.1 % ID/g to 5.2 ±0.1 % ID/g for the BxPC-3 tumor (Δ = − 49 %; $P = 0.0004$). PET/CT images with [^{18}F]AlF **2** in the BxPC-3 model clearly show the uptake in the tumor, along with the primarily renal excretion (Fig. 4). The images also indicate excretion of gastrointestinal radioactivity with the feces at later time points; this was further substantiated by increasing levels of radioactivity observed in fecal biodistribution samples (Supplementary Figure S2).

Discussion

Numerous peptide receptors are significantly overexpressed on the cell surfaces in different tumor types, making radiolabeled peptides promising tools in oncology for diagnosis and treatment [1–5]. For PET imaging, fluorine-18 is a particularly good radioisotope because of its favorable decay characteristics, including a radioactive half-life which aligns well with the biological half-life of peptides. Until recently, peptide radiolabeling with fluorine-18 had to use lengthy multi-step prosthetic group-based chemistries [5–7]. This changed thanks to the development of simple [^{18}F]fluoride-capture reactions, among them radiolabeling with aluminum [^{18}F]fluoride [5, 8–10]. By combining with aluminum chloride, aqueous [^{18}F]fluoride converts to an aluminum [^{18}F]fluoride species which enables simple capture by a NOTA chelator-bearing peptide. Conveniently, NOTA-peptides are accessible through standard peptide chemistry using commercially available reagents and can also be used with diagnostic and therapeutic radiometals [3, 39, 40]. We had previously noted during evaluation of integrin $\alpha_v\beta_6$-targeting analogs of the peptide A20FMDV2 that switching from a covalent prosthetic group (*e.g.*, [^{18}F]FBA) to the ionic [^{18}F]AlF NOTA severely altered the pharmacokinetic profile, especially for the kidneys ([^{18}F]FBA-PEG$_{28}$-A20FMDV2 2.7 ± 0.8 % ID/g *vs.* [^{18}F]AlF NOTA-PEG$_{28}$-A20FMDV2 229 ± 44 % ID/g at 4 h, respectively) [11, 16]. For $\alpha_v\beta_6$-BP, the effect on renal retention was less pronounced ([^{18}F]FBA-$\alpha_v\beta_6$-BP 7.9 ± 2.1 % ID/g *vs.* [^{18}F]AlF **1** 41 ± 10 % ID/g at 4 h, respectively).

Given the promise of the $\alpha_v\beta_6$-BP [33] and the advantages of aluminum [^{18}F]fluoride labeling [8, 10, 13], we decided to further evaluate [^{18}F]AlF **1** and assess the effects of

introducing a moiety capable of non-covalent binding to albumin in the blood stream in order to prolong circulation time and facilitate renal recycling. This approach to improve uptake in target tissue without increasing trapping in kidneys is widely recognized for the improvement of the pharmacokinetic profile of general pharmaceutical drugs [18–24]. It uses a variety of functional groups, including lipids [15], dedicated albumin binding peptides (*e.g.*, the 2.3 kDa SA21; [41]), fragments of albumin binding dyes (*e.g.*, the diazonium dye Evans blue; [28]), or generally small moieties bearing a lipophilic group in proximity to a carboxylic acid [15, 24, 25, 29, 30, 42]. Notable examples with successfully improved pharmacokinetics include magnetic resonance imaging (MRI) contrast agents (*e.g.*, gadofosveset [Ablavar®]; Gd-EOB-DTPA [Primovist®]) [43] and the diabetes drug liraglutide (Victoza®) [19, 24, 44], a synthetic glucagon-like peptide-1 (GLP-1) receptor agonist bearing a palmitoylated γ-glutamyl lysine side chain for albumin binding in order to increase circulation half-life and protect from enzymatic degradation. Taking inspiration from liraglutide's albumin binding structure while forgoing the highly lipophilic palmitic (C-16) acid for the smaller and similarly validated 4-(*p*-iodophenyl)butyric acid [25, 30, 42] and choosing a simple, entirely solid-phase-based synthesis approach, we installed the ABM on the ε-amine of a lysine (Fig. 1). This ABM is a relative of the 4-(*p*-iodophenyl)butyric acid-based albumin-binding structure found by the Neri group [42] and validated by Schibli et al. for radiotracers [25, 26, 30]; conveniently, the installation of our ABM side chain, comprised of an aspartate group separated by a γ-butyrate spacer from the lipophilic 4-(*p*-iodophenyl)butyrate cap (Fig. 1), uses standard Fmoc-peptide chemistry with commercially available reagents for the preparation of NOTA-K(ABM)-$\alpha_v\beta_6$-BP (**2**).

In vitro studies showed that [^{18}F]AlF NOTA-K(ABM)-$\alpha_v\beta_6$-BP ([^{18}F]AlF **2**) did exhibit the anticipated substantial increase in binding to serum protein in ultrafiltration assays compared to the unmodified [^{18}F]AlF NOTA-$\alpha_v\beta_6$-BP ([^{18}F]AlF **1**) and that the binding to human serum protein was slightly stronger than the binding to mouse serum protein; additionally, the albumin binding moiety did not unduly interfere with affinity and selectivity for integrin $\alpha_v\beta_6$ (Fig. 2). Overall, both radiotracers demonstrated moderate to good stability, with some degradation noticed for [^{18}F]AlF **1** in mouse serum. However, as evidenced by the ≥ 95 % unmetabolized [^{18}F]AlF **2** radiotracer after 6 h in human serum, the mouse studies may underestimate the stability in humans because of differences in serum protease composition [45]. *In vivo*, the increased albumin binding of [^{18}F]AlF **2** nearly tripled the fraction of radioactivity retained in the body (Supplementary Figure S1) compared to [^{18}F]AlF **1**. When administered at a constant mass dose of 0.175 nmol/injection—corresponding to 7 nmol/kg for a 25-g mouse and comparable to a typical 3.7 MBq (100 μCi) injection of a metalated radiotracer formulated at 18.5 GBq/μmol (0.5 Ci/ μmol)—high-quality PET scans were obtained 6 h post-injection (Fig. 3) which showed that for [^{18}F]AlF **2**, a considerable amount of radioactivity remained in circulation and that $\alpha_v\beta_6$-directed tumor targeting was clearly visualized in the DX3puroβ6/DX3puro mouse model. Because of this observation, the 6 h biodistribution time point was added for [^{18}F]AlF **2** in favor of the 1 h time point. When comparing the two radiotracers, the biodistribution studies revealed that introduction of the ABM increased the retention in the blood by over two orders of magnitude at 4 h p.i. (Supplementary Table S1), with resulting effects on other tissues (Figs. 3 and 5), notably the DX3puroβ6 tumor for which the uptake more than doubled for [^{18}F]AlF **2** compared to

[^{18}F]AlF **1**, while the kidneys—the organ with the highest uptake for both radiotracers—showed a less than two-fold increase. For both radiotracers, the organs with the next highest uptake were the stomach and intestines. Other tissues also showed increased uptake for [^{18}F]AlF **2**, but notably, uptake in the control tumor, heart, lung, and muscle stayed below that of blood, so this observation may at least partially be explained by radioactivity retained in the blood pool. Given the promising data obtained with [^{18}F]AlF **2** in the DX3puroβ6/DX3puro mouse model which is based on DX3puroβ6 cells engineered to express integrin $\alpha_v\beta_6$, we decided to further study the radiotracer in a model based on endogenous $\alpha_v\beta_6$-expression, specifically the pancreatic BxPC-3 cell line. In this model, the uptake of [^{18}F]AlF **2** in the $\alpha_v\beta_6$-expressing tumor was notably higher than in the engineered DX3puroβ6 tumor. For the pancreatic BxPC-3 tumor xenograft, the tumor uptake continuously increased to13.6 ± 2.5 % ID/g at 6 h post-injection while the pancreas stayed at < 1.2 % ID/g; this, along with the concomitant steady decrease of background signal from radiotracer circulating in the blood pool resulted in clear PET images as late as 6 h post-injection (Fig. 4), thus pointing to the promise of improved radiotracers targeting the integrin $\alpha_v\beta_6$.

Taken together, and in agreement with other published data, this study showed that the introduction of a small albumin binding moiety (ABM) which non-covalently binds to albumin in the bloodstream can be readily carried out on established peptide radiotracers and that the ABM can significantly improve the pharmacokinetic profile (including increased tumor uptake, prolonged circulation, renal recycling) to a point where radiotracers with previously sub-optimal characteristics (such as the aluminum [^{18}F]fluoride-labeled derivatives of the integrin $\alpha_v\beta_6$-targeting peptide A20FMDV2 evaluated here) can compete with or even improve upon their parent compounds. This was demonstrated for [^{18}F]AlF **2** which combines the convenience of [^{18}F]fluoride-capture with improvements of the pharmacokinetic profile compared to its non-albumin binding counterpart [^{18}F]AlF **1**. As clearly seen for the BxPC-3 mouse model, the introduction of the small ABM chosen here for the peptide $\alpha_v\beta_6$-BP can result in a radiotracer that takes several hours to result in the highest accumulation in the target tissue along with clearing of nonspecifically retained activity in urine and feces (Fig. 4, Supplementary Figure S2) (*i.e.*, to achieve maximum target/ background ratio) [24, 25, 28–30]. Consequently, while still beneficial for fluorine-18 radiotracers, the highest tumor uptake with the current ABM may lie beyond the preferred imaging window for fluorine-18 radiotracers (*i.e.*, > 6 h; Fig. 6). Several promising avenues exist for further evaluation, among them the fine-tuning of the albumin binding characteristics through modification of the albumin binding moiety [31, 43, 44, 46] to achieve optimized delivery to the primary target (*i.e.*, integrin $\alpha_v\beta_6$) within the available imaging window, as well as the use of longer-lived diagnostic or therapeutic radioisotopes.

Conclusion

The peptide $\alpha_v\beta_6$-BP selectively targets the cancer-associated integrin $\alpha_v\beta_6$ *in vitro* and *In vivo* and shows great promise as a platform for molecular imaging. NOTA-$\alpha_v\beta_6$-BP is readily radiolabeled with aluminum [^{18}F]fluoride, but the resulting radiotracer could benefit from renal recycling and increased circulation time. Therefore, [^{18}F]AlF NOTA-K(ABM)-$\alpha_v\beta_6$-BP, which still uses convenient aluminum [^{18}F]fluoride radiolabeling but also bears an

albumin binding moiety (ABM), was synthesized and evaluated. Gratifyingly, the modification did not interfere with selectivity or affinity for integrin $\alpha_v\beta_6$, and, in mouse models, resulted in prolonged blood circulation and significantly increased uptake in $\alpha_v\beta_6$-expressing tumors along with comparatively modest effects for organs with major uptake, *i.e.*, kidneys, stomach, and intestines.

Supplementary Material

Refer to Web version on PubMed Central for supplementary material.

Acknowledgments.

We thank the staff of the Center for Molecular and Genomic Imaging (Jennifer Fung, David Kukis, Charles Smith, Sarah Tam, and Josh Waltenburg), David L. Boucher, and Lina Y. Cheuy for technical assistance, scientific support, and discussions.

Funding Information. This study was funded in part by National Institute of Health awards # R01CA211554-01 and R50CA211556-01 and a UC Davis Research Investment in Science and Engineering grant.

References

1. Chatalic KLS, Kwekkeboom DJ, de Jong M (2015) Radiopeptides for imaging and therapy: a radiant future. J Nucl Med 56:1809–1812 [PubMed: 26514175]
2. Okarvi SM, Maecke HR (2018) 17 - Radiolabelled peptides in medical imaging A2 - Koutsopoulos, Sotirios Peptide applications in biomedicine, biotechnology and bioengineering: Woodhead Publishing pp. 431–483
3. Correia JD, Paulo A, Raposinho PD, Santos I (2011) Radiometallated peptides for molecular imaging and targeted therapy. Dalton Trans 40:6144–6167 [PubMed: 21350775]
4. Cives M, Strosberg J (2017) Radionuclide therapy for neuroendocrine tumors. Curr Oncol Rep 19:9 [PubMed: 28220446]
5. Richter S, Wuest F (2014) 18F-labeled peptides: the future is bright. Molecules 19:20536–20556 [PubMed: 25493636]
6. Krishnan HS, Ma L, Vasdev N, Liang SH (2017) 18F-labeling of sensitive biomolecules for positron emission tomography. Chem Eur J 23:15553–15577 [PubMed: 28704575]
7. Vaidyanathan G, Zalutsky MR (2006) Synthesis of N-succinimidyl 4-[18F]fluorobenzoate, an agent for labeling proteins and peptides with 18F. Nat Protoc 1:1655–1661 [PubMed: 17487148]
8. Bernard-Gauthier V, Lepage ML, Waengler B, Bailey JJ, Liang SH, Perrin DM, Vasdev N, Schirrmacher R (2018) Recent advances in 18F radiochemistry: a focus on B-18F, Si-18F, Al-18F, and C-18F radiofluorination via spirocyclic iodonium ylides. J Nucl Med 59:568–572 [PubMed: 29284673]
9. McBride WJ, Sharkey RM, Goldenberg DM (2013) Radiofluorination using aluminum-fluoride (Al18F). EJNMMI Res 3:36 [PubMed: 23651690]
10. Kumar K (2018) 18F-AlF–labeled biomolecule conjugates as imaging pharmaceuticals. J Nucl Med 59:1208–1209 [PubMed: 29880510]
11. Hausner SH, Bauer N, Sutcliffe JL (2014) In vitro and *In vivo* evaluation of the effects of aluminum [18F]fluoride radiolabeling on an integrin alpha(v)beta(6)-specific peptide. Nucl Med Biol 41:43–50 [PubMed: 24267053]
12. Kiesewetter DO, Guo N, Guo J, Gao H, Zhu L, Ma Y, Niu G, Chen X (2012) Evaluation of an [(18)F]AlF-NOTA analog of exendin-4 for imaging of GLP-1 receptor in insulinoma. Theranostics 2:999–1009 [PubMed: 23139727]
13. Kumar K, Ghosh A (2018) 18F-AlF labeled peptide and protein conjugates as positron emission tomography imaging pharmaceuticals. Bioconjug Chem 29:953–975 [PubMed: 29463084]

14. Richter S, Wuest M, Bergman CN, Way JD, Krieger S, Rogers BE, Wuest F (2015) Rerouting the metabolic pathway of18F-labeled peptides: the influence of prosthetic groups. Bioconjug Chem 26:201–212 [PubMed: 25572982]
15. Wetzler M, Hamilton P (2018) 8 - Peptides as therapeutics A2 -Koutsopoulos, Sotirios Peptide applications in biomedicine, biotechnology and bioengineering: Woodhead Publishing pp. 215–230
16. Hausner SH, Kukis DL, Gagnon MKJ, Stanecki CE, Ferdani R, Marshall JF, Anderson CJ, Sutcliffe JL (2009) Evaluation of [64Cu]Cu-DOTA and [64Cu]Cu-CB-TE2A chelates for targeted positron emission tomography with an alpha(v)beta(6)-specific peptide. Mol Imaging 8:111–121 [PubMed: 19397856]
17. Akizawa H, Arano Y, Uezono T, Ono M, Fujioka Y, Uehara T, Yokoyama A, Akaji K, Kiso Y, Koizumi M, Saji H (1998) Renal metabolism of 111In-DTPA-D-Phe1-octreotide *In vivo*. Bioconjug Chem 9:662–670 [PubMed: 9815158]
18. Zhang F, Xue J, Shao J, Jia L (2012) Compilation of 222 drugs' plasma protein binding data and guidance for study designs. Drug Discov Today 17:475–485 [PubMed: 22210121]
19. Sleep D (2014) Albumin and its application in drug delivery. Expert Opin Drug Delivery 12:793–812
20. Dennis MS, Zhang M, Meng YG, Kadkhodayan M, Kirchhofer D, Combs D, Damico LA (2002) Albumin binding as a general strategy for improving the pharmacokinetics of proteins. J Biol Chem 277:35035–35043 [PubMed: 12119302]
21. Lauffer RB, Parmelee DJ, Ouellet HS, Dolan RP, Sajiki H, Scott DM, Bernard PJ, Buchanan EM, Ong KY, Tyeklár Z, Midelfort KS, McMurry TJ, Walovitch RC (1996) MS-325: a small-molecule vascular imaging agent for magnetic resonance imaging. Acad Radiol 3:S356–S358 [PubMed: 8796603]
22. Kratz F (2008) Albumin as a drug carrier: design of prodrugs, drug conjugates and nanoparticles. J Control Release 132:171–183 [PubMed: 18582981]
23. Yamasaki K, Chuang VTG, Maruyama T, Otagiri M (2013) Albumin– drug interaction and its clinical implication. Biochim Biophys Acta Gen Subj 1830:5435–5443
24. Gunnoo SB, Madder A (2016) Bioconjugation – using selective chemistry to enhance the properties of proteins and peptides as therapeutics and carriers. Org Biomol Chem 14:8002–8013 [PubMed: 27461374]
25. Muller C, Struthers H, Winiger C, Zhernosekov K, Schibli R (2013) DOTA conjugate with an albumin-binding entity enables the first folic acid-targeted Lu-177-radionuclide tumor therapy in mice. J Nucl Med 54:124–131 [PubMed: 23236020]
26. Benešová M, Umbricht CA, Schibli R, Müller C (2018) Albumin-binding PSMA ligands: optimization of the tissue distribution profile. Mol Pharm 15:934–946 [PubMed: 29400475]
27. Zhang J, Lang L, Zhu Z, Li F, Niu G, Chen X (2015) Clinical translation of an albumin-binding PET radiotracer 68Ga-NEB. J Nucl Med 56:1609–1614 [PubMed: 26251416]
28. Tian R, Jacobson O, Niu G, Kiesewetter DO, Wang Z, Zhu G, Ma Y, Liu G, Chen X (2018) Evans blue attachment enhances somatostatin receptor subtype-2 imaging and radiotherapy. Theranostics 8:735–745 [PubMed: 29344302]
29. Choy CJ, Ling X, Geruntho JJ, Beyer SK, Latoche JD, Langton-Webster B, Anderson CJ, Berkman CE (2017) 177Lu-labeled phosphoramidate-based PSMA inhibitors: the effect of an albumin binder on biodistribution and therapeutic efficacy in prostate tumor-bearing mice. Theranostics 7:1928–1939 [PubMed: 28638478]
30. Mindt TL, Struthers H, Spingler B, Brans L, Tourwe D et al. (2010) Molecular assembly of multifunctional 99mTc radiopharmaceuticals using "clickable" amino acid derivatives. ChemMedChem 5:2026–2038 [PubMed: 20922747]
31. Kelly JM, Amor-Coarasa A, Nikolopoulou A, Wüstemann T, Barelli P, Kim D, Williams C Jr, Zheng X, Bi C, Hu B, Warren JD, Hage DS, DiMagno SG, Babich JW (2017) Dual-target binding ligands with modulated pharmacokinetics for endoradiotherapy of prostate cancer. J Nucl Med 58:1442–1449 [PubMed: 28450562]

32. Manaenko A, Chen H, Kammer J, Zhang JH, Tang J (2011) Comparison Evans Blue injection routes: intravenous versus intraperitoneal, for measurement of blood–brain barrier in a mice hemorrhage model. J Neurosci Methods 195:206–210 [PubMed: 21168441]
33. Hausner S, Bold RJ, Cheuy LY, Chew HK, Daly ME, et al. (2019) Preclinical development and first-in-human imaging of the integrin αvβ6 with [18F]αvβ6-binding peptide in metastatic carcinoma. Clin Cancer Res 25:1206–1215 [PubMed: 30401687]
34. Bandyopadhyay A, Raghavan S (2009) Defining the role of integrin alpha(v)beta(6) in cancer. Curr Drug Targets 10:645–652 [PubMed: 19601768]
35. Niu J, Li Z (2017) The roles of integrin αvβ6 in cancer. Cancer Lett 403:128–137 [PubMed: 28634043]
36. de Geus SWL, Boogerd LSF, Swijnenburg R-J, Mieog JSD, Tummers WSFJ, Prevoo HAJM, Sier CFM, Morreau H, Bonsing BA, van de Velde CJH, Vahrmeijer AL, Kuppen PJK (2016) Selecting tumor-specific molecular targets in pancreatic adenocarcinoma: paving the way for image-guided pancreatic surgery. Mol Imaging Biol 18:807–819 [PubMed: 27130234]
37. Hausner SH, DiCara D, Marik J, Marshall JF, Sutcliffe JL (2007) Use of a peptide derived from foot-and-mouth disease virus for the noninvasive imaging of human cancer: generation and evaluation of 4-[18F]fluorobenzoyl A20FMDV2 for *In vivo* imaging of integrin alpha(v)beta(6) expression with positron emission tomography. Cancer Res 67:7833–7840 [PubMed: 17699789]
38. Hausner SH, Abbey CK, Bold RJ, Gagnon MK, Marik J, Marshall JF, Stanecki CE, Sutcliffe JL (2009) Targeted *In vivo* imaging of integrin alpha(v)beta(6) with an improved radiotracer and its relevance in a pancreatic tumor model. Cancer Res 69:5843–5850 [PubMed: 19549907]
39. Lee S, Xie J, Chen X (2010) Peptides and peptide hormones for molecular imaging and disease diagnosis. Chem Rev 110:3087–3111 [PubMed: 20225899]
40. Banerjee S, Pillai MRA, Knapp FF (2015) Lutetium-177 therapeutic radiopharmaceuticals: linking chemistry, radiochemistry, and practical applications. Chem Rev 115:2934–2974 [PubMed: 25865818]
41. Pollaro L, Raghunathan S, Morales-Sanfrutos J, Angelini A, Kontos S et al. (2014) Bicyclic peptides conjugated to an albumin-binding tag diffuse efficiently into solid tumors. Mol Cancer Ther 14:151–161 [PubMed: 25381263]
42. Dumelin CE, Trussel S, Buller F, Trachsel E, Bootz F et al. (2008) A portable albumin binder from a DNA-encoded chemical library. Angew Chem Int Ed Engl 47:3196–3201 [PubMed: 18366035]
43. Henoumont C, Laurent S, Muller RN, Elst LV (2012) Effect of nonenzymatic glycosylation on the magnetic resonance imaging (MRI) contrast agent binding to human serum albumin. J Med Chem 55:4015–4019 [PubMed: 22420713]
44. Russell-Jones D (2009) Molecular, pharmacological and clinical aspects of liraglutide, a once-daily human GLP-1 analogue. Mol Cell Endocrinol 297:137–140 [PubMed: 19041364]
45. Jenssen H, Aspmo SI (2008) Serum stability of peptides In: Otvos L (ed) Peptide-based drug design. Humana Press, Totowa, NJ, pp 177–186
46. Umbricht CA, Benešová M, Schibli R, Müller C (2018) Preclinical development of novel PSMA-targeting radioligands: modulation of albumin-binding properties to improve prostate Cancer therapy. Mol Pharm 15:2297–2306 [PubMed: 29684274]

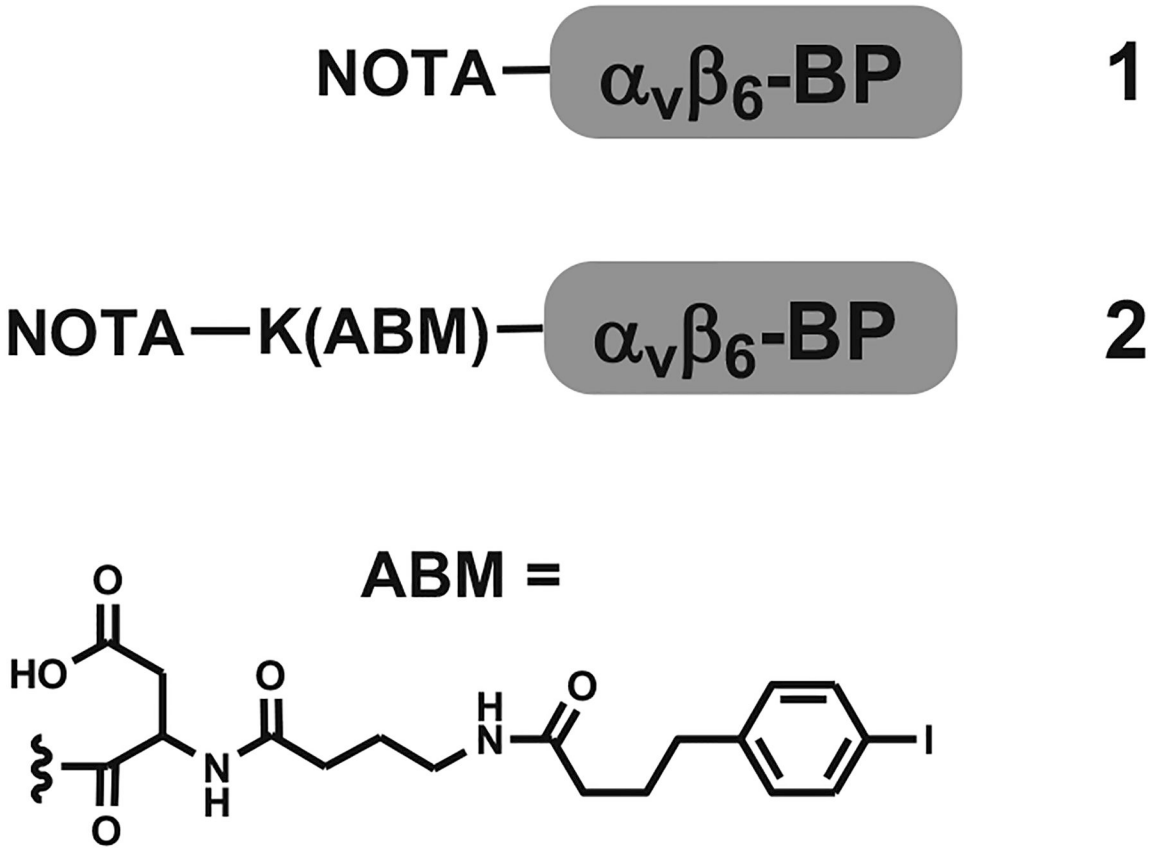

Fig. 1.
Peptides evaluated in this study ($\alpha_v\beta_6$-BP = PEG-NAVPNLRGDLQVLAQRVART-PEG-NH_2).

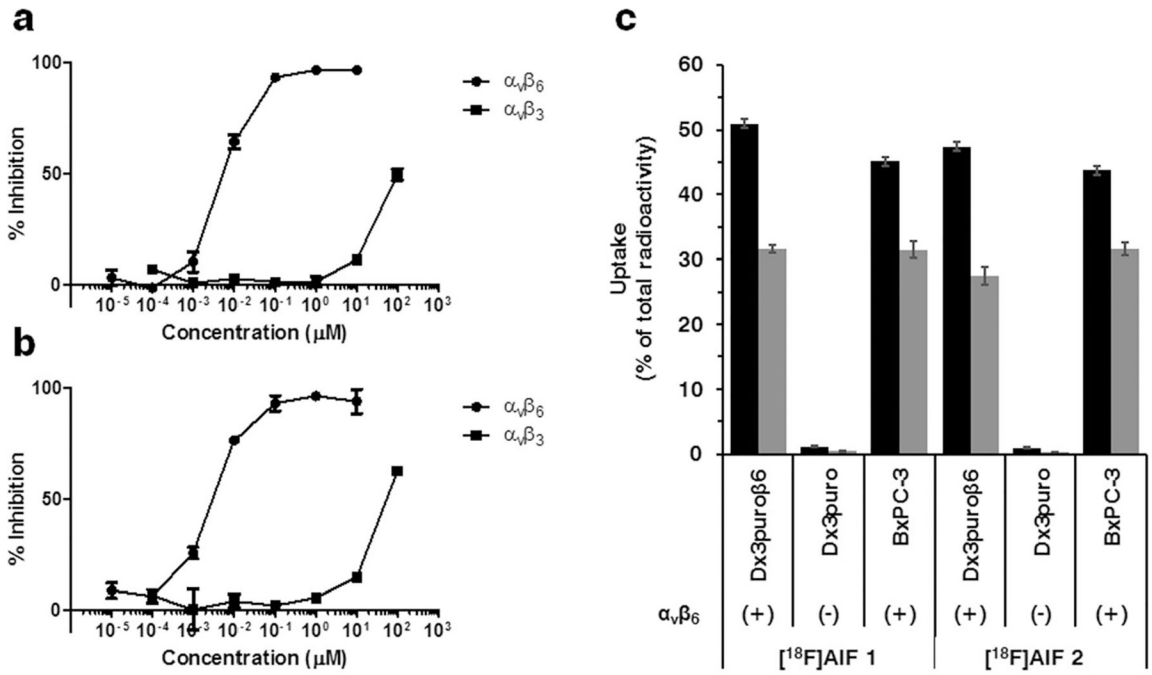

Fig. 2.

In vitro binding experiments. Competitive ELISA of peptides **1** (**a**) and **2** (**b**) for integrins $\alpha_v\beta_6$ and $\alpha_v\beta_3$, respectively (n = 3/peptide/concentration). **c** Cell binding and internalization data of [^{18}F]AlF **1** and [^{18}F]AlF **2** for the integrin $\alpha_v\beta_6$-expressing DX3puroβ6 cells, their paired non-$\alpha_v\beta_6$-expressing DX3puro control, and the $\alpha_v\beta_6$-expressing BxPC-3 cells. Columns: fraction of total radioactivity [%] (n = 4/radiotracer/cell line/condition; 60 min; black: total binding; gray: internalized); bars: SD. DX3puroβ6 *vs.* DX3puro: $P < 1E{-}10$ (total binding, both compounds), $P < 1E{-}8$ (internalization, both compounds).

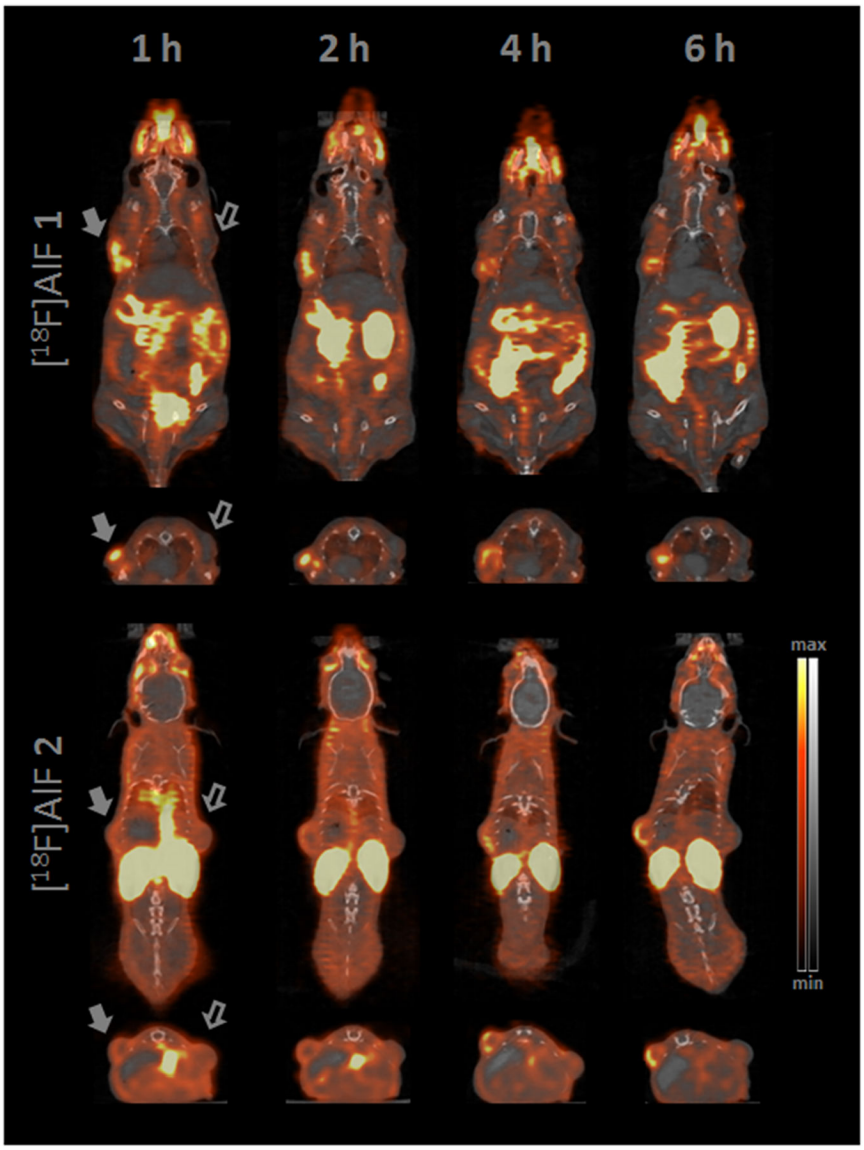

Fig. 3.

Representative coronal and transaxial cross sections of PET/CT images of mice bearing paired DX3puroβ6 [$\alpha_v\beta_6(+)$]/DX3puro [$\alpha_v\beta_6(-)$] xenograft tumors. Both radiotracers were imaged at 1, 2, 4, and 6 h p.i. Filled arrow: DX3puroβ6 tumor, open arrow: DX3puro tumor. Decay corrected PET data are shown in red, CT data in gray.

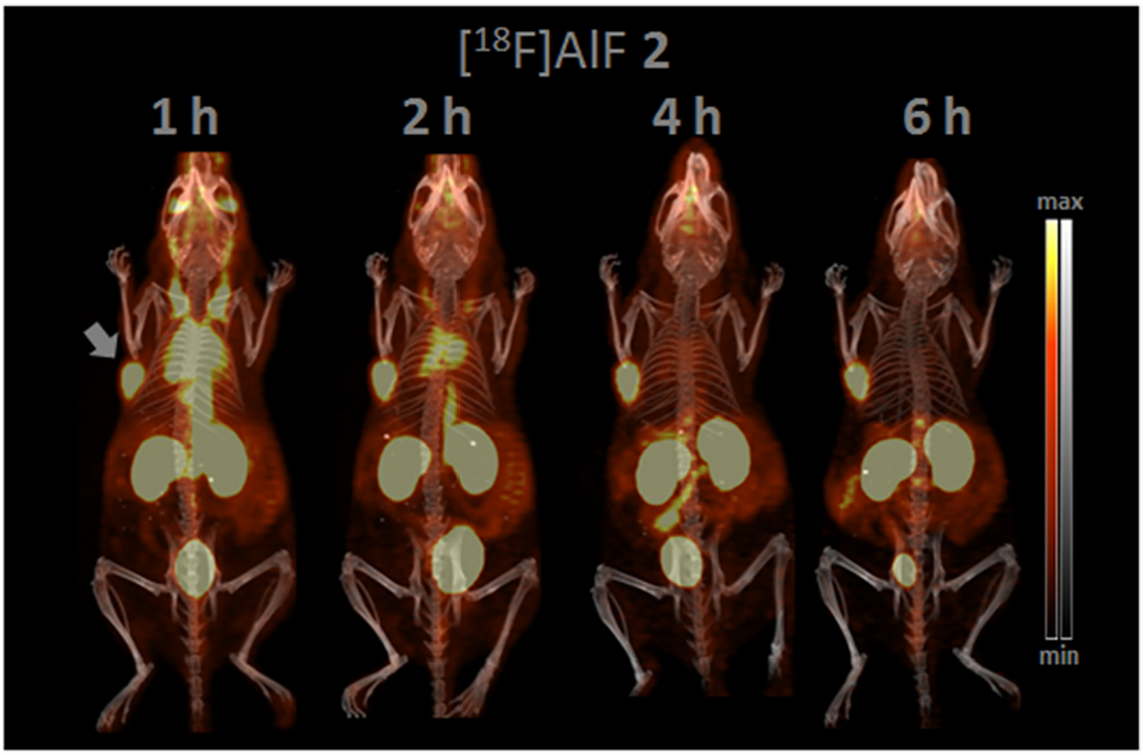

Fig. 4.

Representative maximum intensity projections (MIPs) of PET/CT images of mice bearing BxPC-3 [$\alpha_v\beta_6$(+)] xenograft tumors imaged with [^{18}F]AlF **2** at 1, 2, 4, and 6 h p.i. Filled arrow: tumor. Decay-corrected PET data are shown in red, CT data in gray.

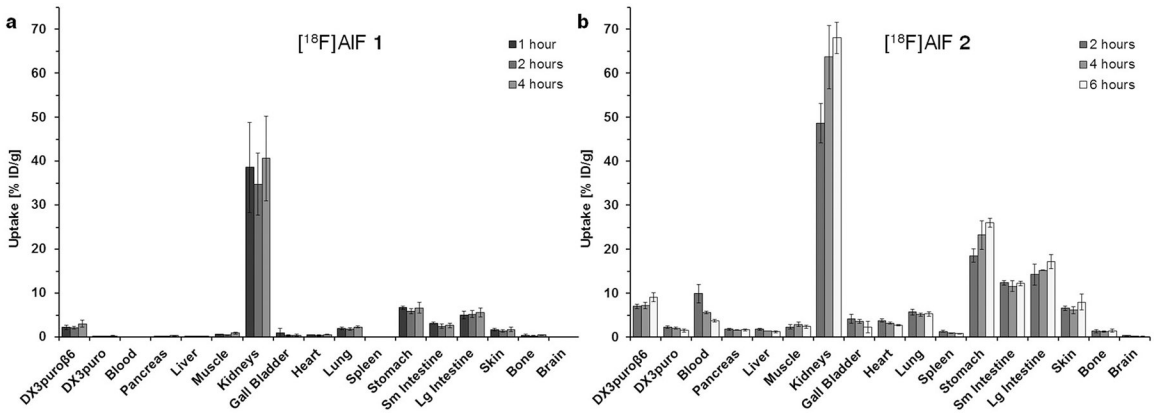

Fig. 5.

Biodistribution data obtained with [^{18}F]AlF **1** (**a**) and [^{18}F]AlF **2** (**b**) in mice bearing paired DX3puroβ6/DX3puro xenograft tumors. Uptake data are expressed as decay-corrected percent of injected dose per gram of tissue (Columns: uptake [% ID/g]; bars: SD; n = 3–4/compound/time point); DX3puroβ6 *vs.* DX3puro: $P < 0.001$ ([^{18}F]AlF **1** and [^{18}F]AlF **2**, all time points).

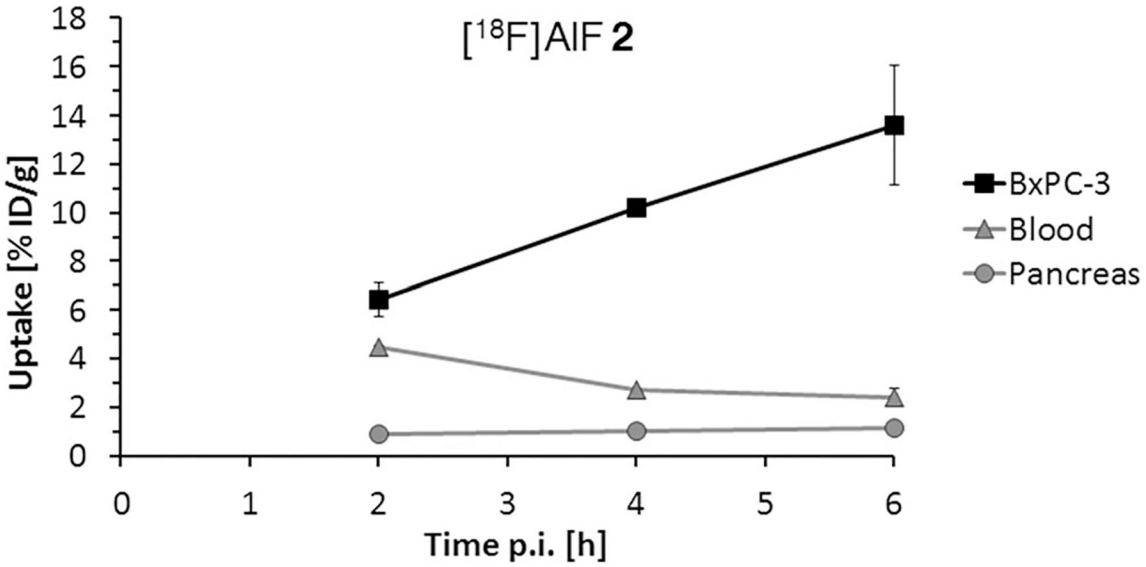

Fig. 6.

Biodistribution time-activity data obtained with [^{18}F]AlF **2** in mice bearing BxPC-3 xenograft tumors. Uptake data are expressed as decay-corrected percent of injected dose per gram of tissue (bars: SD, smaller than the size of the symbol for some data points; n = 3 animals/time point); BxPC-3 *vs.* blood: $P = 0.016$ (2 h), $P = 2E{-}6$ (4 h), $P = 0.0031$ (6 h); BxPC-3 *vs.* pancreas: $P = 0.0003$ (2 h), $P = 5E{-}7$ (4 h), $P = 0.002$ (6 h).